Available online at www.sciencedirect.com
ScienceDirect
Applied Mathematics and Computation 195 (2008) 669–680
APPLIED MATHEMATICS AND COMPUTATION
www.elsevier.com/locate/amc

A power-law model of blood flow through a tapered overlapping stenosed artery

Zuhaila Ismail *, Ilyani Abdullah, Norzieha Mustapha, Norsarahaida Amin

Department of Mathematics, Faculty of Science, Universiti Teknologi Malaysia, 81310 Skudai, Johor, Malaysia

Abstract

A mathematical model of non-Newtonian blood flow through a tapered stenotic artery is considered. The non-Newtonian model chosen is characterized by the generalized power-law model incorporating the effect of tapering due to the pulsatile nature of blood flow. The flow is assumed to be unsteady, laminar, two-dimensional and axisymmetric. The governing equations of motion in terms of the viscous shear stress in the cylindrical coordinate system are solved numerically using a finite difference scheme. Numerical results obtained for the positive taper angle show that the blood flow characteristics such as the axial velocity profiles, flow rate and wall shear stress have lower values, while the resistive impedances have higher values than the Newtonian model.

Keywords: Generalized power-law model; Overlapping stenosis; Tapered artery; Blood flow

1. Introduction

The study of blood flow through a stenosed artery is very important because of the fact that the cause and development of many cardiovascular diseases are related to the nature of blood movement and the mechanical behaviour of the blood vessel walls. A stenosis is defined as a partial occlusion of the blood vessels due to the accumulation of cholesterols and fats and the abnormal growth of tissue. The stenosis is one of the most frequent anomaly in blood circulation. Once the constriction is formed, the blood flow is significantly altered and fluid dynamical factors play important roles as the stenosis continues to enlarge leading to the development of cardiovascular diseases such as heart attack and stroke (Moayeri and Zendehboodi [1]).

A number of theoretical studies related to blood flow through stenosed arteries have been carried out recently and most of the studies focused on the presence of mild or single stenosis as discussed by Chakravarty [2], Chakravarty et al. ([3–5]), Chakravarty and Mandal [6], Taylor et al. [7], Lee and Xu [8] and Mandal [9]. In order to update resemblance to the in vivo situation, some studies considered an overlapping stenosis in the

* Corresponding author.
E-mail addresses: zuhaila@mel.fs.utm.my (Z. Ismail), ilyani@umt.edu.my (I. Abdullah), norzieha@mel.fs.utm.my (N. Mustapha), nsarah@mel.fs.utm.my (N. Amin).

0096-3003/$ - see front matter © 2007 Published by Elsevier Inc.
doi:10.1016/j.amc.2007.05.014

blood vessel segment subject to pulsatile pressure gradient. Chakravarty and Mandal [10] noted that the problem becomes more acute in the presence of an overlapping stenosis in the artery instead of a mild one. The effect of vessel tapering is another important factor that was considered. Chakravarty and Mandal [11] formulated the problem on tapered blood vessel segment having an overlapping stenosis. Jeffords and Knisley [12] and Bloch [13] pointed out that most of the blood vessels could be considered as long and narrow, slowly tapering cones.

In the case of blood flowing through a larger artery, the blood behaviour is acceptable to be assumed as Newtonian. However, it is not valid when the blood vessel is smaller (radius less than 1 mm). From a biofluid mechanics point of view, blood would not be expected to obey the very simple, one parameter, and linearised law of viscosity as developed by Newton. Blood exhibits non-Newtonian characteristics that can only be modelled by higher order constitutive equations, such as the power-law paradigm (Enderle et al. [14]). Ishikawa et al. [16] found that the non-Newtonian pulsatile flow through a stenosed tube is different from Newtonian flow. The non-Newtonian property strengthens the peaks of wall shear stress and wall pressure, weakens the strength of the vortex and reduces the vortex size and separated region. They concluded that non-Newtonian flow is more stable than Newtonian flow. Mandal [9] pointed out that in some disease conditions, for example patients with severe myocardial infarction, cerebrovascular diseases and hypertension, blood exhibits non-Newtonian properties.

Gijsen et al. [15] studied a comparison between the non-Newtonian fluid model and a Newtonian fluid at different Reynolds numbers. Comparison reveals that the character of flow of the non-Newtonian fluid is simulated quite well by using the appropriate Reynolds number. Tu and Deville [17] noticed that for non-Newtonian flow through 75% stenosis, the influence of the geometrical disturbance affects the flow over a longer axial range. Manica and Bortoli [18] presented the simulation of incompressible non-Newtonian flow through channels with sudden expansion using the power-law model. The power-law model is applied to predict pseudoplastic (shear thinning) and dilatant (shear thickening) behaviour in such expansions. They pointed out that a better understanding of non-Newtonian flow through sudden expansions should lead to both the design and development of hydrodynamically more efficient process and to an improved quality control of the final products.

In this paper, we consider the problem of blood flow through an overlapping tapered stenosed artery instead of the mild one as considered by Mandal [9]. The blood flow is characterized by the generalized power-law model. A finite difference scheme is employed to solve the governing equations numerically. A comparison of the velocity profiles and the wall shear stress distributions, together with the flow rate and the resistance to flow distributions are presented for both the Newtonian and non-Newtonian cases.

2. Governing equations

The stenotic blood flow in an arterial segment is considered to be laminar, unsteady, two-dimensional, axisymmetric and fully developed where the flowing blood is treated to be an incompressible fluid. Under these assumptions, the governing equations may be written in the cylindrical coordinates system (r, z, θ) as

Equation of continuity

$$\frac{\partial v_r}{\partial r} + \frac{v_r}{r} + \frac{\partial v_z}{\partial z} = 0. \tag{2.1}$$

Equation of axial momentum

$$\frac{\partial v_z}{\partial t} + v_r \frac{\partial v_z}{\partial r} + v_z \frac{\partial v_z}{\partial z} = -\frac{1}{\rho}\frac{\partial p}{\partial z} - \frac{1}{\rho}\left[\frac{1}{r}\frac{\partial}{\partial r}(r\sigma_{rz}) + \frac{\partial}{\partial z}(\sigma_{zz})\right]. \tag{2.2}$$

Equation of radial momentum

$$\frac{\partial v_r}{\partial t} + v_r \frac{\partial v_r}{\partial r} + v_z \frac{\partial v_r}{\partial z} = -\frac{1}{\rho}\frac{\partial p}{\partial r} - \frac{1}{\rho}\left[\frac{1}{r}\frac{\partial}{\partial r}(r\sigma_{rr}) + \frac{\partial}{\partial z}(\sigma_{rz})\right], \tag{2.3}$$

where the relationship between the shear stress and the shear rate in case of two-dimensional motions are (see Bird et al. [19]):

$$\sigma_{zz} = -2\left\{ m\left|\left[\left(\frac{\partial v_r}{\partial r}\right)^2 + \left(\frac{v_r}{r}\right)^2 + \left(\frac{\partial v_z}{\partial z}\right)^2 + \left(\frac{\partial v_r}{\partial z} + \frac{\partial v_z}{\partial r}\right)^2\right]^{\frac{1}{2}}\right|^{n-1}\right\}\left(\frac{\partial v_z}{\partial z}\right), \tag{2.4}$$

$$\sigma_{rz} = -\left\{ m\left|\left[\left(\frac{\partial v_r}{\partial r}\right)^2 + \left(\frac{v_r}{r}\right)^2 + \left(\frac{\partial v_z}{\partial z}\right)^2 + \left(\frac{\partial v_r}{\partial z} + \frac{\partial v_z}{\partial r}\right)^2\right]^{\frac{1}{2}}\right|^{n-1}\right\}\left(\frac{\partial v_z}{\partial r} + \frac{\partial v_r}{\partial z}\right) \tag{2.5}$$

and

$$\sigma_{rr} = -2\left\{ m\left|\left[\left(\frac{\partial v_r}{\partial r}\right)^2 + \left(\frac{v_r}{r}\right)^2 + \left(\frac{\partial v_z}{\partial z}\right)^2 + \left(\frac{\partial v_r}{\partial z} + \frac{\partial v_z}{\partial r}\right)^2\right]^{\frac{1}{2}}\right|^{n-1}\right\}\left(\frac{\partial v_r}{\partial r}\right). \tag{2.6}$$

Here $v_z(r,z,t)$ and $v_r(r,z,t)$ represent the axial and the radial velocity components, respectively, σ is the stress tensor, p is the pressure, and ρ is the density of blood. The pressure gradient $\partial p/\partial z$ appearing in Eq. (2.1), is given by (see Burton [20])

$$-\frac{\partial p}{\partial z} = A_\circ + A_1 \cos \omega t, \quad t > 0, \tag{2.7}$$

where $A_\circ$ is the constant amplitude of the pressure gradient, A_1 is the amplitude of the pulsatile component giving rise to systolic and diastolic pressure and $\omega = 2\pi f_p$, where f_p is being the pulse frequency.

3. Boundary conditions

There is no radial flow along the axis of the artery and the axial velocity gradient of the streaming blood is assumed to be zero, which means there is no shear rate of fluid along the axis. These may be expressed mathematically as

$$v_r(r,z,t) = 0, \quad \frac{\partial v_z(r,z,t)}{\partial r} = 0, \quad \sigma_{rz} = 0 \quad \text{on } r = 0. \tag{3.1}$$

The velocity boundary conditions on the arterial wall are taken as

$$v_r(r,z,t) = \frac{\partial R}{\partial t}, \quad v_z(r,z,t) = 0 \quad \text{on } r = R(z,t). \tag{3.2}$$

Further, it is assumed that no flow takes places when the system is at rest, which means

$$v_r(r,z,t) = 0 = v_z(r,z,t) \quad \text{at } t = 0. \tag{3.3}$$

4. Geometry of stenosed artery

The schematic diagram for the overlapping stenosis under consideration is shown in Fig. 1.

Following Chakravarty and Mandal [11], the geometry of the elastic (moving wall) arterial wall of the time-variant overlapping stenosis for different taper angles (see Fig. 2) is written mathematically as

$$R(z,t) = \begin{cases} \left[(mz+a) - \frac{\tau_m \cos\phi}{l_0}.(z-d) \times \left\{11 - \frac{94}{3l_0}(z-d) + \frac{32}{l_0^2}(z-d)^2 - \frac{32}{3l_0^3}(z-d)^3\right\}\right] a_1(t); & d \leqslant z \leqslant d + \frac{3l_0}{2}, \\ (mz+a)a_1(t); & \text{otherwise}, \end{cases} \tag{4.1}$$

where $R(z,t)$ denotes the radius of the tapered arterial segment in the constricted region, a, the constant radius of the normal artery in the non-stenotic region, ϕ, the angle of tapering, $3l_0/2$, the length of overlapping stenosis, d, the location of the stenosis, $\tau_m \cos\phi$ is taken to be the critical height of the overlapping stenosis and $m = (\tan\phi)$ represents the slope of the tapered vessel. The arterial segment is taken to be of finite length, L.

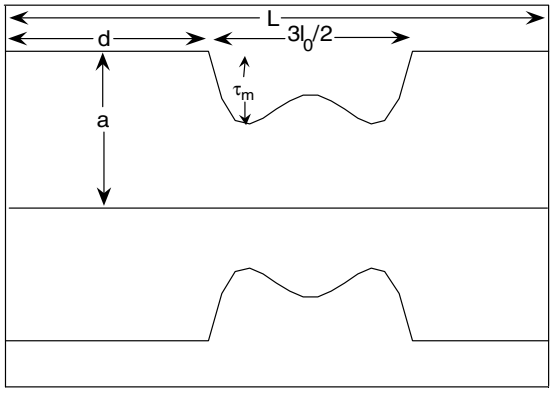

Fig. 1. Schematic diagram of an overlapping stenosed artery.

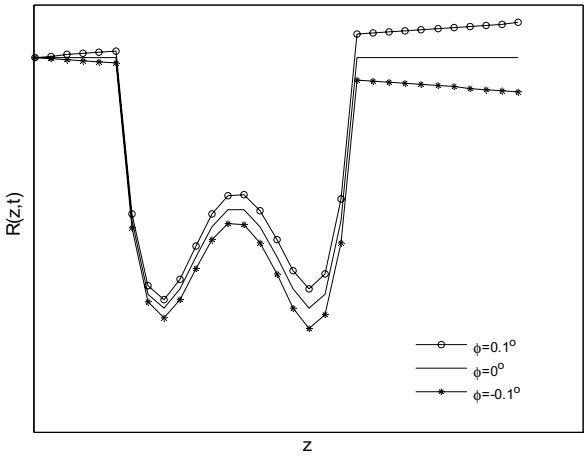

Fig. 2. Schematic diagram of a tapered overlapping stenosed artery.

The time-variant parameter $a_1(t)$ is taken to be

$$a_1(t) = 1 - b(\cos \omega t - 1)\mathrm{e}^{-b\omega t}, \tag{4.2}$$

where b is a constant. Here, the lumen radius, R is sufficiently smaller than the wavelength, λ of the pressure wave i.e. $R/\lambda \ll 1$, Eq. (2.3) simply reduces to $\partial p/\partial r = 0$ and thus Eq. (2.3) can be omitted (see Pedley [21]). It is reasonable and convenient to assume that the pressure is independent of the radial coordinate.

5. Transformation of the governing equations

5.1. Radial coordinate transformation

Using a radial coordinate transformation

$$x = \frac{r}{R(z,t)},$$

which has the effect of immobilizing the vessel wall in the transformed coordinate x, the continuity equation and the equation of motion, (2.1) and (2.2), the relationship between the shear stress and shear rate, (2.4) and (2.5) and the initial and the boundary conditions ((3.1)–(3.3)) become:

Equation of continuity

$$\frac{1}{R}\frac{\partial v_r}{\partial x}+\frac{v_r}{xR}+\frac{\partial v_z}{\partial z}-\frac{x}{R}\frac{\partial v_z}{\partial x}\frac{\partial R}{\partial z}=0. \tag{5.1}$$

Equation of axial momentum

$$\frac{\partial v_z}{\partial t}=\left[\frac{x}{R}\frac{\partial R}{\partial t}-\frac{v_r}{R}+v_z\frac{x}{R}\frac{\partial R}{\partial z}\right]\frac{\partial v_z}{\partial x}-v_z\frac{\partial v_z}{\partial z}-\frac{1}{\rho}\frac{\partial p}{\partial z}-\frac{1}{\rho}\left[\frac{1}{xR}\sigma_{xz}+\frac{1}{R}\frac{\partial \sigma_{xz}}{\partial x}+\frac{\partial \sigma_{zz}}{\partial z}-\frac{x}{R}\frac{\partial \sigma_{xz}}{\partial x}\frac{\partial R}{\partial z}\right]. \tag{5.2}$$

Equation of normal stress, (σ_{zz})

$$\sigma_{zz}=-2\left\{m\left|\left[\left(\frac{1}{R}\frac{\partial v_r}{\partial x}\right)^2+\left(\frac{v_r}{xR}\right)^2+\left(\frac{\partial v_z}{\partial z}-\frac{x}{R}\frac{\partial R}{\partial z}\frac{\partial v_z}{\partial x}\right)^2+\left(\frac{\partial v_r}{\partial z}-\frac{x}{R}\frac{\partial R}{\partial z}\frac{\partial v_r}{\partial x}+\frac{1}{R}\frac{\partial v_z}{\partial x}\right)^2\right]^{\frac{1}{2}}\right|^{n-1}\right\}\left(\frac{\partial v_z}{\partial z}-\frac{x}{R}\frac{\partial R}{\partial z}\frac{\partial v_z}{\partial x}\right). \tag{5.3}$$

Equation of shear stress, (σ_{xz})

$$\sigma_{xz}=-\left\{m\left|\left[\left(\frac{1}{R}\cdot\frac{\partial v_r}{\partial x}\right)^2+\left(\frac{v_r}{xR}\right)^2+\left(\frac{\partial v_z}{\partial z}-\frac{x}{R}\frac{\partial R}{\partial z}\frac{\partial v_z}{\partial x}\right)^2+\left(\frac{\partial v_r}{\partial z}-\frac{x}{R}\frac{\partial R}{\partial z}\frac{\partial v_r}{\partial x}+\frac{1}{R}\frac{\partial v_z}{\partial x}\right)^2\right]^{\frac{1}{2}}\right|^{n-1}\right\}\left(\frac{1}{R}\frac{\partial v_z}{\partial x}+\frac{\partial v_r}{\partial z}-\frac{x}{R}\frac{\partial R}{\partial z}\frac{\partial v_r}{\partial x}\right), \tag{5.4}$$

where n is the fluid behaviour index parameter.

Boundary conditions

$$v_r(x,z,t)=0,\quad \frac{\partial v_z(x,z,t)}{\partial x}=0,\quad \sigma_{rz}=0\quad \text{on } r=0, \tag{5.5}$$

$$v_r(x,z,t)=\frac{\partial R}{\partial t},\quad v_z(x,z,t)=0\quad \text{on } x=R(z,t) \tag{5.6}$$

and

$$v_r(x,z,t)=0=v_z(x,z,t)\quad \text{at } t=0. \tag{5.7}$$

5.2. The radial momentum

In order to obtain the radial velocity component, $v_r(x,z,t)$, we multiply Eq. (5.1) by xR, then integrate the equation with respect to x from the limits $0\to x$, to obtain

$$v_r=x\frac{\partial R}{\partial z}v_z-\frac{R}{x}\int_0^x x\frac{\partial v_z}{\partial z}\,dx-\frac{2}{x}\frac{\partial R}{\partial z}\int_0^x xv_z\,dx. \tag{5.8}$$

Using the boundary condition (5.6), Eq. (5.8) takes the following form

$$-\int_0^1 x\frac{\partial v_z}{\partial z}\,dx=\frac{1}{R}\frac{\partial R}{\partial t}+\frac{2}{R}\frac{\partial R}{\partial z}\int_0^1 xv_z\,dx. \tag{5.9}$$

Since the choice of $f(x)$ is arbitrary, let $f(x)$ be of the form

$$f(x)=4(1-x^2)$$

with $f(x)$ satisfying

$$\int_0^1 xf(x)\,dx=1.$$

Now, Eq. (5.9), can be rewritten as

$$-\int_0^1 x\frac{\partial v_z}{\partial z}\,dx=\int_0^1 xf(x)\frac{1}{R}\frac{\partial R}{\partial t}\,dx+\frac{2}{R}\frac{\partial R}{\partial z}\int_0^1 xv_z\,dx=\int_0^1 x\left[\frac{2}{R}\frac{\partial R}{\partial z}v_z+\frac{1}{R}\frac{\partial R}{\partial t}f(x)\right]dx. \tag{5.10}$$

Comparing the left hand side and right hand side of Eq. (5.10) and substituting $f(x)$ into the above equation, we obtain

$$\frac{\partial v_z}{\partial z} = -\frac{2}{R}\frac{\partial R}{\partial z}v_z + \frac{4}{R}(x^2-1)\frac{\partial R}{\partial t}. \tag{5.11}$$

Then, substituting Eq. (5.11) into Eq. (5.8), gives the radial velocity component as

$$v_r(x,z,t) = x\left[\frac{\partial R}{\partial z}v_z - \frac{\partial R}{\partial t}[2-x^2]\right]. \tag{5.12}$$

6. Numerical procedure

The finite difference scheme for solving Eq. (5.1) is based on the central difference approximations for all the first spatial derivatives in the following manner:

$$\frac{\partial v_z}{\partial x} = \frac{(v_z)^k_{i,j+1} - (v_z)^k_{i,j-1}}{2\Delta x} \quad \text{and} \quad \frac{\partial v_z}{\partial z} = \frac{(v_z)^k_{i+1,j} - (v_z)^k_{i-1,j}}{2\Delta z}, \tag{6.1}$$

while the time derivative in Eq. (5.1) is approximated by

$$\frac{\partial v_z}{\partial t} = \frac{(v_z)^{k+1}_{i,j} - (v_z)^k_{i,j}}{\Delta t}. \tag{6.2}$$

Similarly, the derivatives for v_r, σ_{zz} and σ_{xz} are

$$\frac{\partial v_r}{\partial x} = \frac{(v_r)^k_{i,j+1} - (v_r)^k_{i,j-1}}{2\Delta x} \quad \text{and} \quad \frac{\partial v_r}{\partial z} = \frac{(v_r)^k_{i+1,j} - (v_r)^k_{i-1,j}}{2\Delta z}, \tag{6.3}$$

$$\frac{\partial \sigma_{zz}}{\partial x} = \frac{(\sigma_{zz})^k_{i,j+1} - (\sigma_{zz})^k_{i,j-1}}{2\Delta x}, \quad \frac{\partial \sigma_{zz}}{\partial z} = \frac{(\sigma_{zz})^k_{i+1,j} - (\sigma_{zz})^k_{i-1,j}}{2\Delta z} \quad \text{and} \quad \frac{\partial \sigma_{xz}}{\partial x} = \frac{(\sigma_{xz})^k_{i,j+1} - (\sigma_{xz})^k_{i,j-1}}{2\Delta x}. \tag{6.4}$$

The discretization of $v_z(x,z,t)$ is written as $v_z(x_j,z_i,t_k)$ where it can be written as $(v_z)^k_{i,j}$. Here, we define

$$x_j = (j-1)\Delta x; \quad j = 1,2,\ldots N+1 \quad \text{where } x_{N+1} = 1.0,$$
$$z_i = (i-1)\Delta z; \quad i = 1,2,\ldots M+1,$$
$$t_k = (k-1)\Delta t; \quad k = 1,2,\ldots$$

Using Eqs. (6.1)–(6.4), the discretized form of Eqs. (5.1), (5.3) and (5.4) are given as:

$$(v_z)^{k+1}_{i,j} = (v_z)^k_{i,j} + \Delta t\left\{\left[\frac{x_j}{R^k_i}\left(\frac{\partial R}{\partial t}\right)^k_i - \frac{(v_r)^k_{i,j}}{R^k_i} + (v_z)^k_{i,j}\frac{x_j}{R^k_i}\left(\frac{\partial R}{\partial z}\right)^k_i\right]\left(\frac{\partial v_z}{\partial x}\right)^k_{i,j} - (v_z)^k_{i,j}\left(\frac{\partial v_z}{\partial z}\right)^k_{i,j} - \frac{1}{\rho}\left(\frac{\partial p}{\partial z}\right)^{k+1} - \frac{1}{\rho}\left[\frac{1}{x_j R^k_i}(\sigma_{xz})^k_{i,j} + \frac{1}{R^k_i}\left(\frac{\partial \sigma_{xz}}{\partial x}\right)^k_{i,j} + \left(\frac{\partial \sigma_{zz}}{\partial z}\right)^k_{i,j} - \frac{x_j}{R^k_i}\left(\frac{\partial \sigma_{xz}}{\partial x}\right)^k_{i,j}\left(\frac{\partial R}{\partial z}\right)^k_i\right]\right\}, \tag{6.5}$$

$$(\sigma_{zz})^k_{i,j} = -2\left\{m\left|\left[\left(\frac{1}{R^k_i}\left(\frac{\partial v_r}{\partial x}\right)^k_{i,j}\right)^2 + \left(\frac{(v_r)^k_{i,j}}{x_j R^k_i}\right)^2 + \left(\left(\frac{\partial v_z}{\partial z}\right)^k_{i,j} - \frac{x_j}{R^k_i}\left(\frac{\partial R}{\partial z}\right)^k_i\left(\frac{\partial v_z}{\partial x}\right)^k_{i,j}\right)^2 + \left(\left(\frac{\partial v_r}{\partial z}\right)^k_{i,j} - \frac{x_j}{R^k_i}\left(\frac{\partial R}{\partial z}\right)^k_i\left(\frac{\partial v_r}{\partial x}\right)^k_{i,j} + \frac{1}{R^k_i}\left(\frac{\partial v_z}{\partial x}\right)^k_{i,j}\right)^2\right]^{\frac{1}{2}}\right|^{n-1}\right\}\left(\left(\frac{\partial v_z}{\partial z}\right)^k_{ij} - \frac{x_j}{R^k_i}\left(\frac{\partial R}{\partial z}\right)^k_i\left(\frac{\partial v_z}{\partial x}\right)^k_{ij}\right), \tag{6.6}$$

$$(\sigma_{xz})^k_{i,j} = -\left\{m\left|\left[\left(\frac{1}{R^k_i}\left(\frac{\partial v_r}{\partial x}\right)^k_{i,j}\right)^2 + \left(\frac{(v_r)^k_{i,j}}{x_j R^k_i}\right)^2 + \left(\left(\frac{\partial v_z}{\partial z}\right)^k_{i,j} - \frac{x_j}{R^k_i}\left(\frac{\partial R}{\partial z}\right)^k_i\left(\frac{\partial v_z}{\partial x}\right)^k_{i,j}\right)^2 + \left(\left(\frac{\partial v_r}{\partial z}\right)^k_{i,j} - \frac{x_j}{R^k_i}\left(\frac{\partial R}{\partial z}\right)^k_i\left(\frac{\partial v_r}{\partial x}\right)^k_{i,j} + \frac{1}{R^k_i}\left(\frac{\partial v_z}{\partial x}\right)^k_{i,j}\right)^2\right]^{\frac{1}{2}}\right|^{n-1}\right\}\left(\left(\frac{\partial v_r}{\partial z}\right)^k_{i,j} - \frac{x_j}{R^k_i}\left(\frac{\partial R}{\partial z}\right)^k_i\left(\frac{\partial v_r}{\partial x}\right)^k_{i,j} + \frac{1}{R^k_i}\left(\frac{\partial v_z}{\partial x}\right)^k_{i,j}\right). \tag{6.7}$$

The discretized boundary conditions ((5.5)–(5.7)) are

$$(v_r)_{i,j}^k = 0, \quad (v_z)_{i,1}^k = (v_z)_{i,2}^k, \quad (\sigma_{xz})_{i,1}^k = 0, \tag{6.8}$$

$$(v_z)_{i,N+1} = 0, \quad (v_r)_{i,N+1}^k = \left(\frac{\partial R}{\partial t}\right)_i^k \tag{6.9}$$

and

$$(v_r)_{i,j}^1 = 0, \quad (v_z)_{i,j}^1 = 0. \tag{6.10}$$

The axial velocity component will be solved using the Eqs. (6.6) and (6.7), together with the boundary conditions Eqs. ((6.8)–(6.10)). The radial velocity component from Eq. (5.12) can be rewritten in discretized form as

$$(v_r)_{i,j}^{k+1} = x_j \left[\left(\frac{\partial R}{\partial z}\right)_i^k (v_z)_{i,j}^{k+1} - \left(\frac{\partial R}{\partial t}\right)_i^k [2 - x_j^2] \right]. \tag{6.11}$$

The radial velocity component can be calculated directly from Eq. (6.11), using the result of the axial velocity component. With the above results, we obtain the volumetric flow rate (Q), the resistance to flow (Ω), the wall shear stress (τ_w) from the following relations:

$$Q_i^k = 2\pi (R_i^k)^2 \int_0^1 x_j (v_z)_{i,j}^k \, \mathrm{d}x_j, \tag{6.12}$$

$$\Omega_i^k = \frac{|L(\partial p/\partial z)^k|}{Q_i^k}, \tag{6.13}$$

$$(\tau_w)_i^k = \mu \left[\frac{1}{R_i^k} \left(\frac{\partial v_z}{\partial x}\right)_{i,j}^k + \left(\frac{\partial v_r}{\partial z}\right)_{i,j}^k - \frac{x_j}{R_i^k} \left(\frac{\partial v_r}{\partial x}\right)_{i,j}^k \left(\frac{\partial R}{\partial z}\right)_i^k \right]_{x=1} \times \cos \left[\arctan \left(\frac{\partial R}{\partial z}\right)_i^k \right]. \tag{6.14}$$

7. Numerical results and discussion

There are different methods of solution in solving the problem of blood flow in stenosed artery, either analytically or numerically. Gerrard and Taylor [22] used the finite difference method to solve the problem of blood flow in an artery. The finite difference method based on the central difference approximation has been employed by Chakravarty and Mandal ([23,6]) and Mandal [9]. Misra and Pal [24] observed the blood motion using Crank Nicolson implicit finite difference method, while Chakravarty and Mandal ([10,11]), Chakravarty et al. ([3–5]) and Chakravarty and Sannigrahi [25] used Runge–Kutta.

For the purpose of validation, the axial velocity profile for Newtonian model with $\phi = 0^\circ$ is compared with Chakravarty and Mandal [11]. As shown in Fig. 3, the results are found to be in good agreement. Numerical computations have been carried out using the following parameter values: $a = 0.05$ cm, $\rho = 1.06$ g/cm^3, $L = 5$ cm, $l_0 = 1$ cm, $d = 2$ cm, $\tau_m = 0.2a$, $A_0 = 50$ g cm^{-2} s^{-2}, $A_1 = 0.2A_0$, $f_p = 1.2$ Hz, $\mu = 0.035P$, $b = 0.1$, $m = 0.1735P$, $n = 0.639$, $\Delta x = 0.025$, and $\Delta z = 0.1$. For the numerical results and discussion, Figs. 4–7 and Figs. 9–11 have been measured at the location of the first critical height of stenosis (at $z = 2.3$ cm with $\tau_m = 0.01$ cm). The blood is assumed to be in the early stage of diastole phase for a single cardiac cycle when the time reaches 0.45 s where the flow is at minimum. The results in Figs. 4, 5 and 8 are measured at this phase of flow. Figs. 6–8 give the results for converging tapered artery ($\phi = -0.1^\circ$) and for the Newtonian viscosity model, we consider the diverging tapered artery ($\phi = 0.1^\circ$).

Fig. 4 shows the axial velocity profiles in the stenotic region of the tapered artery. Four different curves shown in Fig. 4, have been measured with the effects of vessel tapering for non-Newtonian model of the flow on the axial velocity profiles quantitatively. Under stenotic conditions, the velocities through the converging tapered artery are less than those in the non-tapered artery and the diverging tapered artery. Hence, we can conclude that the axial velocity is reduced to some extent with vessel tapering. As shown in Fig. 4, another point of comparison is the different blood viscosity models. In the presence of the diverging artery under stenotic conditions, the axial velocity is higher in the Newtonian model than in the non-Newtonian model.

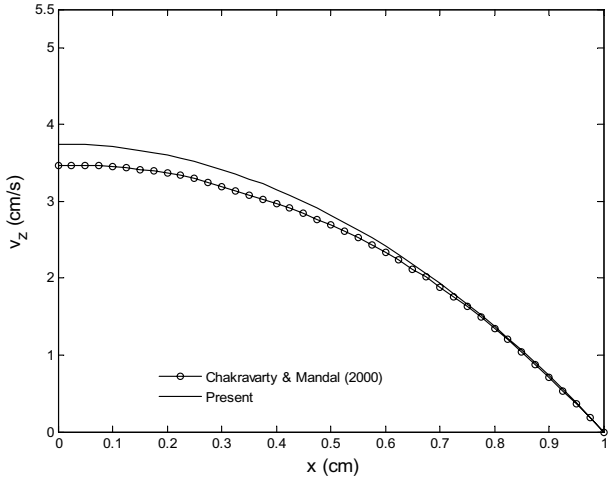

Fig. 3. Axial velocity profile at $z = 1.0$ cm for $t = 0.25$ s.

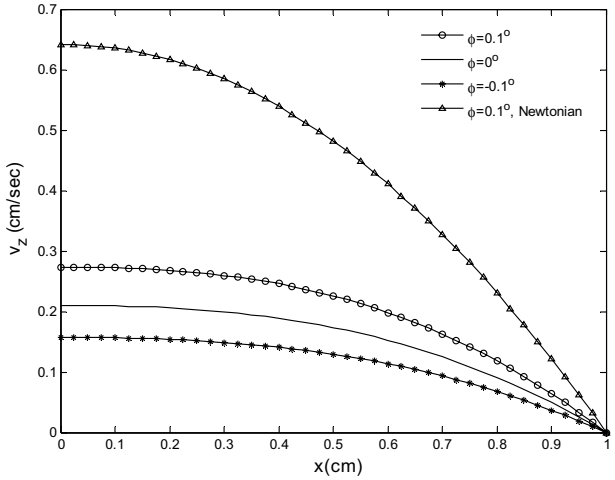

Fig. 4. Axial velocity profile at $z = 2.3$ cm for $t = 0.45$ s.

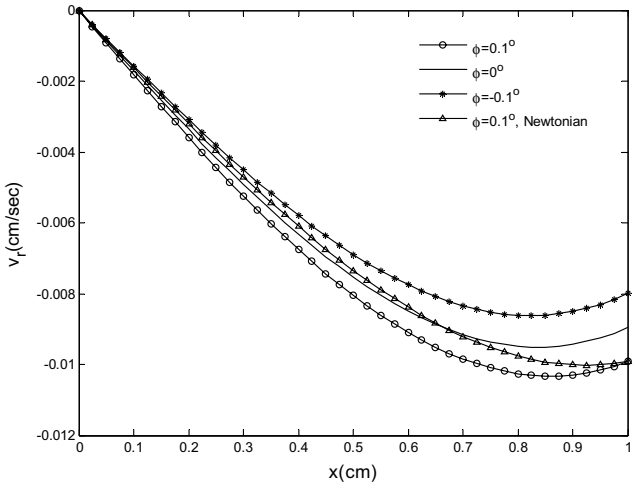

Fig. 5. Radial velocity profile at $z = 2.3$ cm for $t = 0.45$ s.

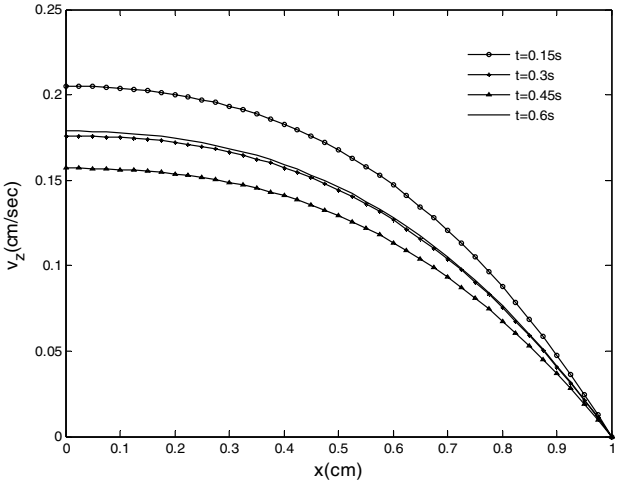

Fig. 6. Axial velocity profile at different times with $z = 2.3$ cm through converging artery ($\phi = -0.1^\circ$).

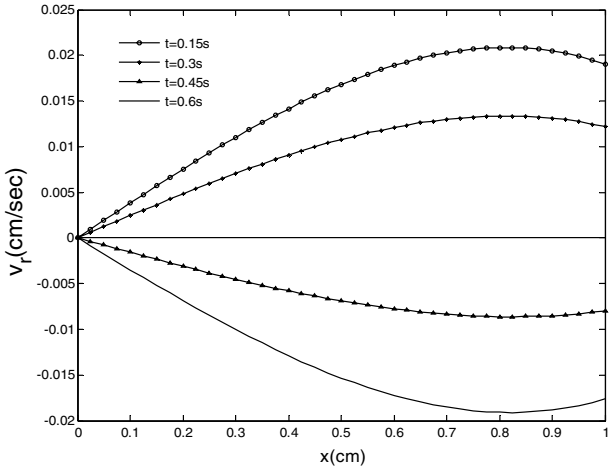

Fig. 7. Radial velocity profile at different times with $z = 2.3$ cm through converging artery ($\phi = -0.1^\circ$).

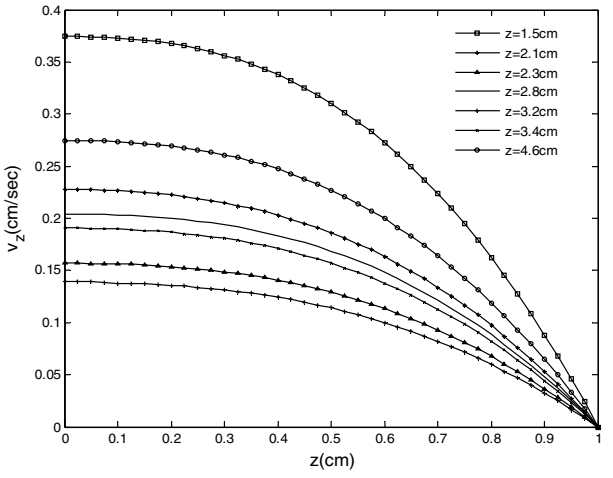

Fig. 8. Axial velocity profile for different axial locations through converging artery ($\phi = -0.1^\circ$) for $t = 0.45$ s.

A plot of the radial velocity profiles is shown in Fig. 5 for the same characteristics of the axial velocity profiles. The results for radial velocity give four different negative values with the effect of tapering artery and blood viscosity. The magnitudes of the radial velocities are smaller than the axial velocities.

Fig. 6 shows the result for the axial velocity profiles for different times spread over a single cardiac period. All the profiles visualized in the present figure are directly responsible for the pulsatile pressure gradient produced by the heart. A full single cardiac cycle is about 0.85 s. thus, at $t = 0.45$ s, the blood volume is minimum and the axial velocity profiles are the lowest.

Fig. 7 illustrates the unsteady flow over a single cardiac cycle. It shows that the radial velocity profiles have positive values during the systolic phase while during the diastolic phase, the profiles give negative values.

In order to analyze the flow-field intensively along the arterial segment, Fig. 8 shows the result of the axial velocity profiles at seven distinct locations at $t = 0.45$ s for converging tapered artery ($\phi = -0.1^\circ$). The axial velocity profile is parabolic at the upstream ($z = 1.5$ cm) because it is a non-stenotic region while a flattening trend is followed at $z = 2.1$ cm where the blood flow starts at a steeper stenosis region. Subsequently, at the specific location ($z = 2.3$ cm) of the first critical height of the stenosis, the velocity value is much lower. At the centre of the overlapping location ($z = 2.8$ cm), the velocity value is increased but it is decreased when the blood flow along the second critical height ($z = 3.2$ cm). The axial velocity value increases gradually for $z = 3.4$ cm and finally at the downstream of stenosis ($z = 4.6$ cm), the value is increased and gets back into the parabolic shape. This result is agreed qualitatively well with Chakravarty and Mandal [11] which they treated the blood flow as a Newtonian fluid.

Figs. 9–11 are plotted for the flow rate, the resistance to flow and the wall shear stress, respectively, with time nearly four cardiac cycles. Fig. 9 shows the profiles for flow rate in stenosed artery with three different taper angles. The volume rate for diverging tapering gives higher value than both the converging tapering and non-tapered artery. The figure also shows that for Newtonian model, the flow rate has the highest value.

The resistance to flow gives the reverse trend of the volume rate. The values of resistance are higher for converging tapering artery rather than both the converging artery and non-tapered artery and lower for the Newtonian viscosity model as shown in Fig. 10. From Figs. 9 and 10, we can conclude that more blood can flow freely through diverging vessel, which has less effect of resistance.

Fig. 11 illustrates the wall shear stress profiles for different taper angles and the different blood viscosity models. The values are negative by direction. From the first three curves, we can observe that diverging tapering gives higher values compared to both the converging tapering and non-tapered artery. Fig. 11 also shows the wall shear stress values are higher in the Newtonian model than in the non-Newtonian model.

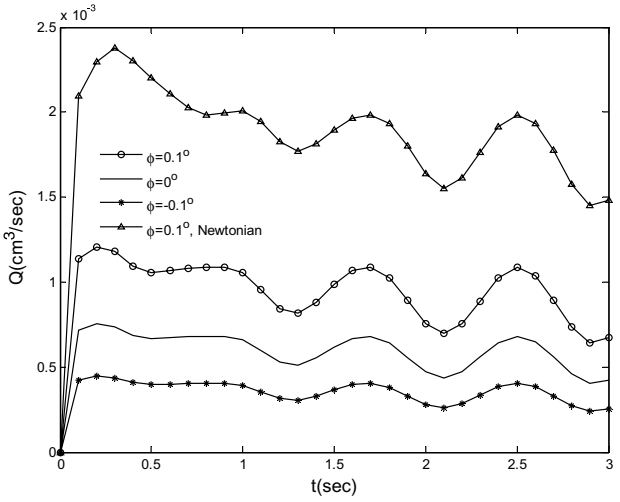

Fig. 9. Variation of the flow rate at $z = 2.3$ cm.

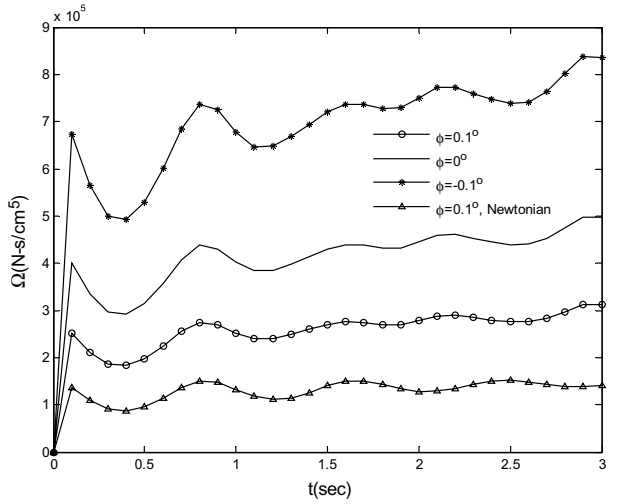

Fig. 10. Variation of the resistance to flow at $z = 2.3$ cm.

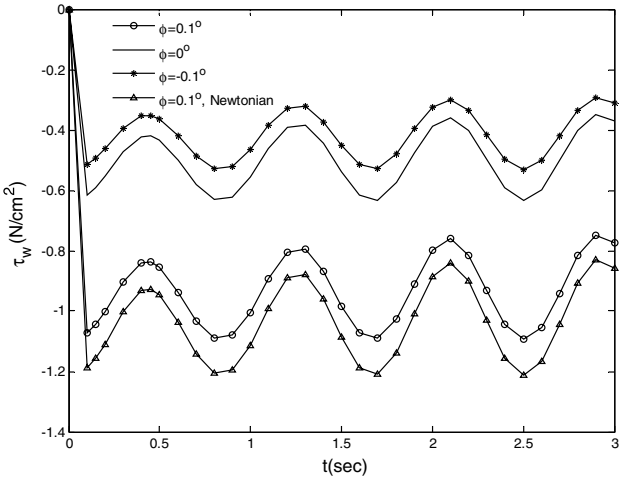

Fig. 11. Variation of the wall shear stress at $z = 2.3$ cm.

8. Conclusions

This paper presented numerical results for an unsteady blood flow in a tapered artery with overlapping stenosis, using the power-law model of blood viscosity. The effect of vessel tapering is an important factor considered in this paper. The results considered three different taper angles of artery which are the converging tapering ($\phi < 0^\circ$), non-tapered ($\phi = 0^\circ$) and the diverging tapering ($\phi > 0^\circ$) in the presence of stenosis. The differences between both models show that the non-Newtonian behaviour is an important factor and should not be neglected in small blood vessels (smaller than 1 mm).

Acknowledgements

We would like to thank to Dr. Prashanta Kumar Mandal from Visva-Bharati, India for his invaluable suggestions that lead to the improvement of this paper and to JPA (SLAB), UTM and KUSTEM for financial support.

References

[1] M.S. Moayeri, G.R. Zendehboodi, Effect of elastic property of the wall on flow characteristics through arterial stenosis, Journal of Biomechanics 36 (2003) 525–535.
[2] S. Chakravarty, Effect of stenosis on the flow behaviour of blood in an artery, International Journal of Engineering Science 25 (1987) 1003–1018.
[3] S. Chakravarty, A. Datta, A.K. Mandal, Analysis of nonlinear blood flow in a stenosed flexible artery, International Journal of Engineering Science 33 (1995) 1821–1837.
[4] S. Chakravarty, A. Datta, A.K. Mandal, Effect of body acceleration on unsteady flow of blood past a time-dependent arterial stenosis, Mathematical and Computer Modelling 24 (1996) 57–74.
[5] S. Chakravarty, P.K. Mandal, A. Mandal, Mathematical model of pulsatile flow in a distensible aortic bifurcation subject to body acceleration, International Journal of Engineering Science 38 (2000) 215–238.
[6] S. Chakravarty, P.K. Mandal, An analysis of pulsatile flow in a model aortic bifurcation, International Journal of Engineering Science 35 (1997) 409–422.
[7] C.A. Taylor, T.J.R. Hughes, C.K. Zarins, Finite element modeling of blood flow in arteries, Computer Methods in Applied Mechanics and Engineering 158 (1998) 155–196.
[8] K.W. Lee, X.Y. Xu, Modelling of flow and wall behaviour in a mildly stenosed tube, Medical Engineering & Physics 24 (2002) 575–586.
[9] P.K. Mandal, An unsteady analysis of non-newtonian blood flow through tapered arteries with a stenosis, International Journal of Non-Linear Mechanics 40 (2005) 151–164.
[10] S. Chakravarty, P.K. Mandal, A nonlinear two-dimensional model of blood flow in an overlapping arterial stenosis subjected to body acceleration, Mathematical and Computer Modelling 24 (1996) 43–58.
[11] S. Chakravarty, P.K. Mandal, Two-dimensional blood flow through tapered arteries under stenotic conditions, International Journal of Non-Linear Mechanics 35 (2000) 779–793.
[12] J.V. Jeffords, M.H. Knisley, Concerning the geometric shapes of arteries and arteriols, Angiology 7 (1956) 105–136.
[13] E.H. Bloch, A quantitative study of the themodynamics in the living microvascular system, American Journal of Anatomy 110 (1962) 125–153.
[14] J. Enderle, B. Susan, B. Bronzino, Introduction to Biomedical Engineering, Academic Press, London, 2000.
[15] F.J.H. Gijsen, E. Allanic, F.N. Vosse, J.D. Janssen, The influences of the non-newtonian properties of blood on the flow in large arteries: unsteady flow in a 90° curved tube, Journal of Biomechanics 32 (1999) 705–713.
[16] T. Ishikawa, L.F.R. Guimaraes, S. Oshima, R. Yamone, Effect of non-newtonian property of blood on flow through a stenosed tube, Fluid Dynamic Research 22 (1998) 251–264.
[17] C. Tu, M. Deville, Pulsatile flow of non-newtonian fluids through arterial stenoses, Journal of Biomechanics 29 (1996) 899–908.
[18] R. Manica, A.L. Bortoli, Simulation of incompressible non-newtonian flows through channels with Suddens expansion using the power-law model, Tema – Tendências em Matemática Aplicada e Computacional 4 (2003) 333–340.
[19] R.B. Bird, W.E. Stewart, E.N. Lightfoot, Transport Phenomena, Wiley International Edition, 1960.
[20] A.C. Burton, Physiology and Biophysics of the Circulation. Introductory Text, Year Book Medical Publisher, Chicago, 1966.
[21] T.J. Pedley, The Fluid Mechanics of Large Blood Vessels, Cambridge University Press, London, 1980.
[22] J.H. Gerard, L.A. Taylor, Mathematical model representing blood flow in arteries, Medical & Biological Engineering & Computing 15 (1977) 611–617.
[23] S. Chakravarty, P.K. Mandal, Mathematical modelling of blood flow through an overlapping arterial stenosis, Mathematical and Computer Modelling 19 (1994) 59–70.
[24] J.C. Misra, B. Pal, A mathematical model for the study of the pulsatile flow of blood under an externally imposed body acceleration, Mathematical and Computer Modelling 29 (1999) 89–106.
[25] S. Chakravarty, A.K. Sannigrahi, A nonlinear mathematical model of blood flow in a constricted artery experiencing body acceleration, Mathematical and Computer Modelling 29 (1999) 9–25.